International Journal of Multiphase Flow 35 (2009) 699–709

Contents lists available at ScienceDirect

International Journal of Multiphase Flow

journal homepage: www.elsevier.com/locate/ijmulflow

Flow pattern and boiling heat transfer of CO_2 in horizontal small-bore tubes

Mamoru Ozawa *, Takeyuki Ami, Isao Ishihara, Hisashi Umekawa, Ryosuke Matsumoto, Yasuhiko Tanaka, Taku Yamamoto, Yuya Ueda

Department of Mechanical Engineering, Kansai University, 3-3-35 Yamate-cho, Suita, Osaka 564-8680, Japan

ARTICLE INFO

Article history:
Received 6 January 2009
Received in revised form 21 March 2009
Accepted 2 April 2009
Available online 12 April 2009

Keywords:
Flow boiling
Flow pattern
Mini-channel
Carbon dioxide
Discrete bubble model

ABSTRACT

Increasing attention has been focused on carbon dioxide (CO_2) heat pump system where the temperature level is rather low, while the operating pressure is rather high. In this system, the density difference between vapor and liquid becomes rather small, which significantly affects flow patterns. Low surface tension and latent heat also have significant influence on two-phase flow patterns and heat transfer. This paper describes experimental and numerical investigation on flow patterns and heat transfer characteristics of boiling flow CO_2 at high pressure in horizontal small-bore tubes ranging from 1.0 mm to 3.0 mm I.D. Even though the density difference is rather small at high pressure, phase stratification takes place, which leads to the intermittent dryout at the upper wall. So far developed discrete bubble model by the authors for vertical flows is modified so as to include horizontal flow mechanisms. The predicted flow patterns with this new model agree on the whole with the experimental observation.

1. Introduction

Natural refrigerants, such as ammonia, isobutene and carbon dioxide, have attracted attention in air conditioning and refrigeration technologies. Carbon dioxide (CO_2, p_{cr} = 7.383 MPa, T_{cr} = 31.1 °C) among them has incombustibility and non-toxicity, and in addition, is not in need to recover. Thus special emphasis is recently put on a CO_2 heat pump application. The heat transfer performance of CO_2 is as high as other refrigerants, while operating at rather high pressure covering the trans-critical pressure region. To develop compact heat exchanger for the CO_2 heat pump system, a mini-channel heat exchanger is preferably used because of its high specific heat-transfer-area. In terms of thermo-physical properties of CO_2, the viscosity is small being preferable in application to mini-channel, which results in low pressure drop but with high heat transfer coefficient (Park and Hrnjak, 2007). Aiming at such application, extensive works have been so far conducted on flow boiling CO_2 (e.g. Thome and Ribatski, 2005; Schael and Kind, 2005; Cheng et al., 2008) and two-phase flow in micro- and mini-channels (e.g. Mishima and Hibiki, 1995; Kandlikar, 2002; Kandlikar and Grande, 2003; Thome, 2006a, 2006b; Revellin and Thome, 2006). The boiling two-phase flow and heat transfer in mini-channel, however, have not been sufficiently understood for the heat exchanger application.

In this study, experiments were extensively conducted with small-bore tubes of 1.0 mm, 2.0 mm and 3.0 mm to investigate the flow pattern, the heat transfer performance including the effects of tube size, the system pressure and the mass flux on the boiling heat transfer of CO_2. As the detailed discussion on the heat transfer characteristics and the pressure drop may be found elsewhere (Yamamoto et al., 2007; Ozawa, 2009), here in this paper the flow patterns and the related heat transfer phenomenon, "intermittent dryout", are mainly focused. The flow pattern maps obtained in the experiment are compared with the existing criteria as well as the predicted results with the discrete bubble model developed by the authors. And then the regime-based modeling of slug flow is applied to demonstrate principal mechanism of the intermittent dryout, so that the behavior of time-averaged heat transfer coefficient is well interpreted.

2. Experimental apparatus

Schematic diagram of the experimental apparatus is shown in Fig. 1. Liquid CO_2 supplied from a cylinder is fed through a pump, a buffer tank, a pre-cooler, and is regulated via an expansion valve so as to retain the predetermined pressure. Then, the liquid CO_2 flows successively through a heated section, an adiabatic section and a sight glass, and is finally released to the atmosphere after the mass flow measurement with a laminar flowmeter.

The heated and the adiabatic sections are made of SUS304 horizontal tubes. The tube inner diameters covered in this experiment are D_p = 1.0 mm (2.0 mm O.D.), 2.0 mm (3.96 mm O.D.) and 3.0 mm (4.01 mm O.D.), as listed in Table 1 together with experimental conditions. Each tube is designated as 1-mm tube, 2-mm tube and 3-mm tube, respectively, for convenience. AC power was supplied to the heated tube for Joule heating, and the outer wall

* Corresponding author. Tel./fax: +81 6 6368 0807.
E-mail address: ozawa@ipcku.kansai-u.ac.jp (M. Ozawa).

0301-9322/$ - see front matter © 2009 Elsevier Ltd. All rights reserved.
doi:10.1016/j.ijmultiphaseflow.2009.04.003

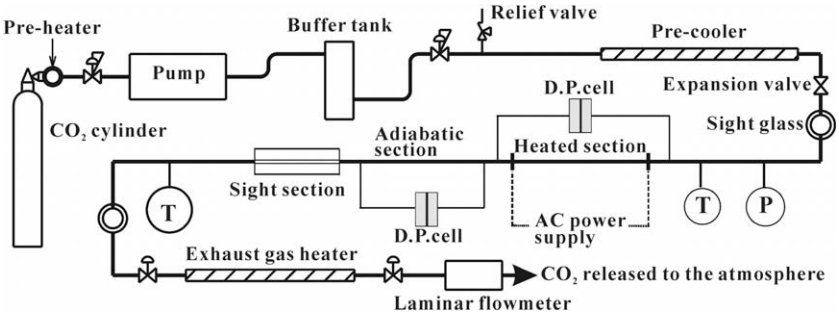

Fig. 1. Schematic of experimental system (*T*: thermocouple, *P*: pressure gauge).

Table 1
Experimental condition.

D_p (mm)	1.0	2.0	3.0
p (MPa)	4.0–6.7	5.0–6.7	4.5–6.5
T_S (°C)	5.3–26.8	22.0–26.8	10.0–25.4
L_H (mm)	800	1850	1700
G (kg/m^{2}s)	200–700	200–500	100–300
q (kW/m^2)	10–50	5–35	5–25
ΔT_{sub} (K)	1–13	9–17	5–10

D_p: tube diameter, p: pressure, T_S: saturated temperature, L_H: heated length, G: mass flux, heat flux, ΔT_{sub}: inlet subcooling.

temperatures were measured at every 100 mm along the heated tube both on the upper and lower walls with K-type thermocouples (accuracy 0.1 K) of 0.025 mm (for 1-mm tube) and 0.1 mm (for 2-mm and 3-mm tubes) in diameter. The adiabatic section was used only for the pressure drop measurement, otherwise removed. The pressure drop measurement was conducted by means of a differential pressure transducer with a measurement error less than 0.075% of full scale (0–50 kPa). The pressure transducer used in this experiment had an accuracy of 0.5%. The accuracy of the flow rate was around 1.5% of full scale. The temperatures and the pressure drops were recorded simultaneously via data acquisition system. The heat transfer coefficient was calculated by using time-averaged value of 120 data of the measured temperatures. All the test section and the adiabatic section were thermally insulated, while the saturation temperatures in most of the cases were around the room temperature, even slightly lower at low pressure, and thus a heat loss or heat intrusion from the ambient were almost negligible. The sight sections were made of a quartz glass with inner diameters of 1.0 mm, 2.0 mm and 3.0 mm, and outer diameter of 16 mm. The two-phase flow pattern was recorded by a digital camera and a high-speed video-camera.

The dimensional tolerance of inner diameter may have a significant influence on the experimental data in a small-bore tube. The inner diameter was measured with a microscope and the surface roughness of the inner wall was detected by using a laser microscope and a tracer method. The roughness on the inner walls were at most 8 μm, and the single-phase friction factor well coincided with the Hagen–Poiseuille equation in laminar flow and with the Blasius equation in turbulent flow. Thus the tube inner walls were considered hydraulically smooth enough.

3. Flow pattern

Typical flow patterns in 2-mm tube at 5.0 MPa and 6.5 MPa are shown in Fig. 2 as a function of vapor quality and mass flux. The present discussion is conducted focussing on the 2-mm tube, while covers whole range of experimental findings including the results

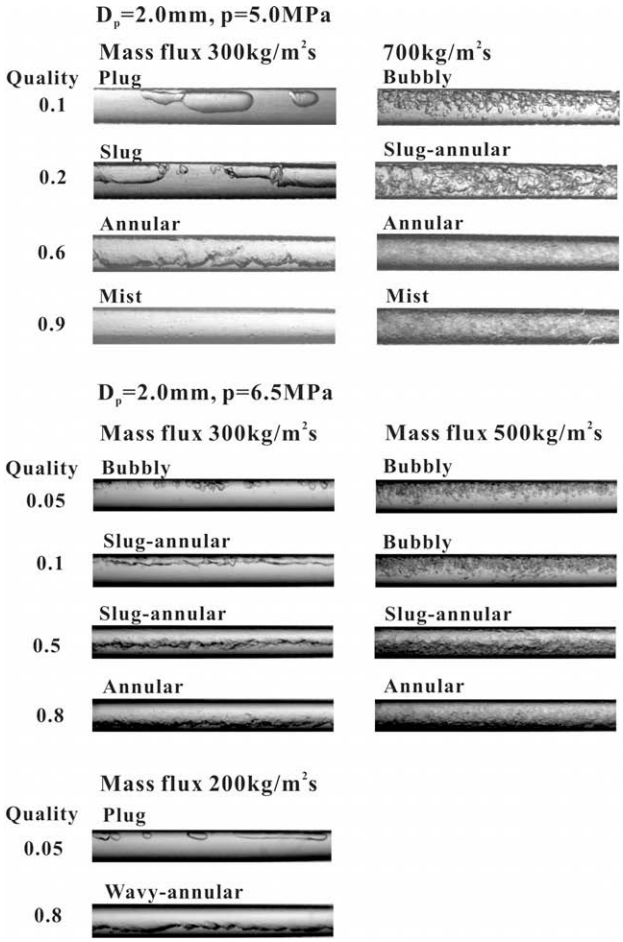

Fig. 2. Observed flow pattern of CO_2, D_p = 2.0 mm.

in 1-mm and 3-mm tubes. Thus some typical flow patterns and flow pattern maps are contained in the Appendix for reference.

The observed flow patterns are characterized as follows:

Bubbly flow: dispersed small bubbles or cloud of small bubbles,
Plug flow: elongated slow-moving bubbles with relatively low void fraction,
Slug flow: intermittent large-scale liquid lumps, i.e. liquid slugs, and large bubbles,
Annular flow: gas core, often with entrainments, surrounded with liquid film,
Mist flow: dispersed small droplets or mist,
Wavy flow: stratified flow with wavy interface,

Slug–annular flow: gas flow penetrating through the liquid slug, which includes churn flow in the classification of Triplett et al. (1999),

Wavy–annular flow: annular flows with thick and wavy liquid layer at the bottom, and

Wavy–mist flow: wavy flow with liquid entrainment above the liquid layer.

The first six categories are almost consistent with the conventional-sized tube, i.e. macro-channel, while the last three are all transition categories between slug-to-annular, wavy-to-annular and wavy-to-mist, respectively.

The flow patterns observed in the 2-mm tube at 5.0 MPa (density ratio $\rho_L/\rho_G = 827.9/156.6 = 5.28$) are quite similar to macro-channels, while in 1.0-mm tube as shown in Fig. A1, the geometrical configuration of, typically, slug flow is clearly different from that in 2-mm tube, i.e. the gas–liquid interface or large bubble shape is seemingly axi-symmetric, and is close to those observed by Serizawa et al. (2002) with a micro-channel of 20–100 μm in diameter. There exists no substantial difference on flow configuration between 2-mm and 3-mm tubes.

At higher pressure, i.e. 6.5 MPa, $\rho_L/\rho_G = 703.6/248.3 = 2.83$, the flow pattern in 1-mm tube becomes more like macro-channel with special reference to the phase-stratification tendency. The flow patterns in 2-mm and 3-mm tubes are still close to macro-channel mode, while vapor–liquid interface becomes even smooth at higher pressure like a thin thread of vapor, as typically shown in 3-mm tube at low mass flux (ref. Fig. A2). It is worthy to note that even at such a high pressure, phase stratification or effect of gravity dominates the flow pattern. This is typically exemplified with an existence of wavy, wavy–annular or wavy–mist flows in 2-mm and 3-mm tubes at low mass flux and high quality.

Supposing an air–water system near atmospheric pressure, the flow pattern essentially becomes axi-symmetric as Triplett et al. (1999) for micro-channel of 1.1–1.45 mm in diameter and Serizawa et al. (2006) for 20–100 μm due to the effect of surface tension even with a large density difference between gas and liquid. In the present experiment, such axi-symmetric flow pattern was observed only in 1-mm tube at 5.0 MPa, and the cases otherwise were more like macro-channels in their geometrical configurations, as shown in the flow pattern at 6.5 MPa even in the case of 1-mm tube (ref. Fig. A1). This may be caused by a weak effect of surface tension of high-pressure CO_2 relative to the effect of gravity. The combined effects of these parameters and the tube dimensions may be scaled with the help of the Bond number as given below.

The flow pattern maps of 2-mm tube are shown in Fig. 3. The solid lines are transition boundaries given by Cheng et al. (2008), which is a revised version of Thome and El Hajal (2003) for ca. 8–14 mm in diameter, based on the CO_2 data from smaller-bore to ordinarily sized tube, being also a revised version of Kattan et al. (1998) for ca. 10- to 12-mm tubes. Thus the map by Cheng et al. (2008) is applicable to macro-channels. Comparing the observed flow pattern at 5.0 MPa with the transition curves by Cheng et al. (2008), the bubbly and intermittent flows including plug and slug flows are nearly involved in or close to the respective region, while the slug–annular flow regime penetrates into the predicted annular flow region. The annular flow region extends toward lower quality at high mass flux, and the mist flow appears reasonably at high quality. In the case of 3-mm tube, the data are rather limited within rather low mass flux, plug flow and a part of slug flow involved in the predicted intermittent region. Another flow pattern transition shown by dashed lines of Revellin and Thome's (2007) for micro-channel, are drawn as well. Over-all feature is consistent with those predicted, i.e. the bubbly and plug

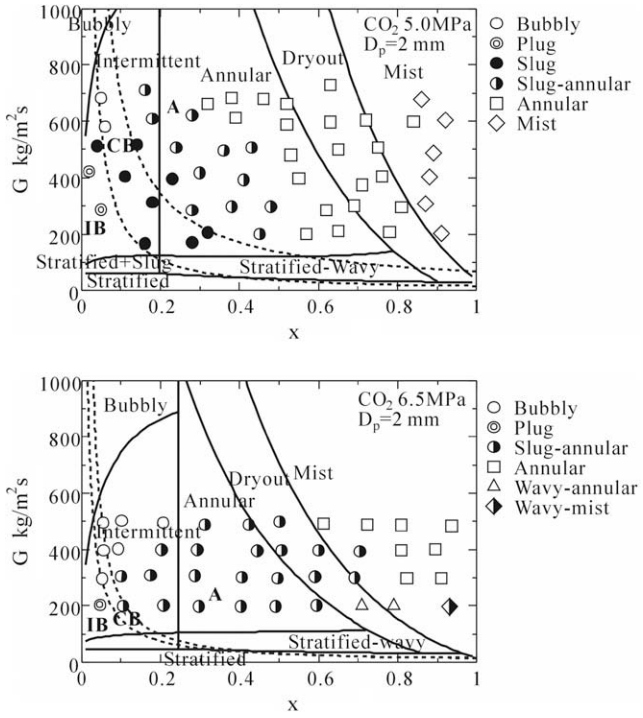

Fig. 3. Flow pattern map of CO_2 in 2-mm tube. Solid lines: Cheng et al. (2008) and dashed lines: Revellin and Thome (2006), IB: isolated bubble, CB: coalescing bubble, A: annular flow.

flows well corresponds to *isolated bubble (IB)* regime, and *coalescing bubble (CB)* regime well includes the slug flow. The slug to slug–annular boundary well corresponds to *coalescing bubble-to-annular (CB-A)* boundary, while the transition mode, i.e. slug–annular, is not considered in the Revellin and Thome's flow pattern criteria. This is also the case in 1-mm tube (see Fig. A3).

Referring to the map for 6.5 MPa, the bubbly flow region expands toward lower mass flux, while the slug flow is not observed in 2-mm tube. Instead, the slug–annular regime extends toward lower and higher quality regions, which is not the case of 1-mm tube. The bubbly and intermittent flows in 1-mm tube agree with the boundary of Cheng et al., while not in 2-mm tube. The wavy–annular flow and wavy–mist appeared at low mass flux and high quality, which may correspond to the stratified–wavy regime of Cheng et al. (2008). The flow pattern prediction by Revellin and Thome's is not appropriate throughout the examined tubes.

In viewing the flow patterns maps including Figs. A3 and A4 in the Appendix, it is suggested that all the examined tubes ranging 1.0–3.0 mm show, at lower pressure, similar characteristics to the micro-channel with respect to an agreement with the IB and CB boundaries of Revellin and Thome (2007) for micro-channel, and show, at higher pressure, macro-channel characteristics of an appearance of wavy, wavy–annular or wavy–mist flow. The agreement, even though a limited part, with the Revellin and Thome's diagram, however, does not simply mean a similarity with micro-channel mode in the geometrical configuration. The geometrical configurations or phase distribution in the tube cross section, being an important factor in heat transfer phenomena, show consistently the macro-channel characteristics, except the case at 5 MPa in 1-mm tube in the present experiment. In this respect, the flow of CO_2 in 1-mm tube at 5 MPa is classified as or close to the micro-channel flow and those in 2 mm- and 3-mm tubes as well as 1-mm tube at higher pressure, 6.5 MPa, are classified as the macro-channel flow.

The criteria for micro-mini-macro classification of flow have been given with various parameters. The simplest one is the Kandlikar's criterion (Kandlikar, 2002; Kandlikar and Grande, 2003) with tube diameter D_p,

$$\begin{aligned} &\text{Macro-channel}: \ 3.0\ \text{mm} < D_p \\ &\text{Mini-channel}: \ 200\ \mu\text{m} < D_p < 3.0\ \text{mm} \\ &\text{Micro-channel}: \ D_p < 200\ \mu\text{m} \end{aligned} \tag{1}$$

This criterion might be deduced based on the experimental observation with air–water and/or refrigerant at relatively low pressure. Based on the present flow pattern observation at high pressure, where the density ratio is close to unity, the criterion may be modified so as to include fundamental flow mechanisms. When a horizontal flow is the case, one of the important features, having a substantial influence on the heat transfer, is the phase stratification, leading to a difference in heat transfer at the upper and lower walls of the tube.

Kew and Cornwell (1997) proposed the threshold diameter between macro-to-micro tubes given as a function of the Bond number Bd by

$$Bd \equiv \frac{\rho_{LG} g D_p^2}{\sigma} = 4 \tag{2}$$

where g denotes the gravitational acceleration, $\rho_{LG} = \rho_L - \rho_G$ the density difference between gas and liquid, σ the surface tension. The gravity force tends to enhance phase stratification and the surface tension force promotes axi-symmetric geometry of the interface especially in a narrow channel. Fig. 4 represents the simplified boundary by Kandlikar (2002) and the boundary predicted with Eq. (2) for CO_2 as a function of pressure. Based on the concept by Kew and Cornwell (1997), 0.5-mm and 1-mm tube, used so far conducted experiment by Yamamoto et al. (2007), are included in the range suffering from a significant influence of geometrical confinement and surface tension below 5 MPa, while the 1-mm tube suffers less influence above 6 MPa. Actually, the 1-mm tube is very close to the macro-to-micro boundary. The present 2-mm and 3-mm tubes belong to the macro-channel group beyond 4.5 MPa. The flow patterns shown in Fig. 2 and maps support this classification.

Schael and Kind (2005) presented flow pattern map of CO_2 obtained in D_p = 8.62-mm tube at p = 3.97 and 2.64 MPa with micro-fin on a inner surface. Although the pressure level of their experiment is lower than the present case, the slug–annular regime penetrates into the predicted annular flow region similarly to the present case, and moreover the flow pattern map by Schael and Kind is on the whole similar to the present 2-mm tube data, which also support that 2-mm tube is included in the macro-tube category. Based on Eq. (2), Schael and Kind's data range in Bond number from 104 to 161. In cases of air–water system, on the other hand, the Bond number becomes 0.132 in 1-mm tube, and reaches only just 2 in 4-mm tube. Triplett et al. (1999) belongs to this range. Weisman's diagram (Weisman et al., 1979) is based on macro-channels ranging 11.5–94 mm and the Bond number ranges 17–1170, although Weisman's intermittent-annular boundary is close to Revellin and Thomes's curve for 5.0 MPa CO_2.

As described above, so far proposed flow pattern transition criteria have a difficulty in predicting slug–annular flow being a quite important in interpreting the intermittent dryout at the upper wall as described below. In this regard, the presented data of the flow patterns of high-pressure CO_2 may be useful in possible improvements of the transition criteria. In this paper, however, alternative approach, i.e. pattern dynamics approach, is conducted to realize void fraction fluctuation pattern, so that the flow pattern identification becomes possible based on a statistical properties of void fraction fluctuation, similarly to Jones and Zuber (1975).

4. Pattern dynamics approach to horizontal two-phase flow

Authors have developed a pattern dynamics model being referred to as "discrete bubble model" aiming to simulate inherent fluctuation of two-phase flow (Ozawa et al., 2007; Ami et al., 2007). This model applied to an isothermal vertical flow has been verified in statistical and time-averaged characteristics of two-phase flow. The discrete bubble model consists of a mass conservation equation of gas phase and a limited number of momentum effects, and has a possibility of a variety of applications. An application to a horizontal two-phase flow is also one of the cases. As the detailed description of the model may be found elsewhere (Ami et al., 2008), here in this paper only a draft is described in the followings.

The discrete bubble model is constructed based on the frame of reference, being referred to as unit cell in this paper, having a dimension of tube diameter D_p as illustrated in Fig. 5. Then the two-phase flow is represented as a series of discrete bubbles, having a geometrical similarity with the unit cell, along the tube, where only one bubble of D_b in diameter and also in length is defined in each cell. Then the void fraction ε_G is given simply by $\varepsilon_G = (D_b/D_p)^3$. In the figure, p denotes pressure, and i the cell number. Applying the void propagation equation, i.e. mass conservation equation of gas phase, as a global rule, bubble movement is traced with the help of several local rules demonstrating momentum contributions, e.g. a volume expansion by pressure change, a wake

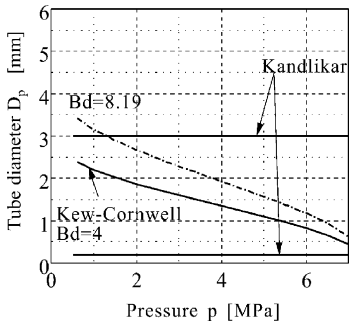

Fig. 4. Boundaries of macro-to-micro channel by Kandlikar (2002) and Kew and Cornwell (1997).

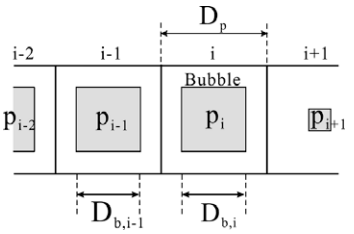

Fig. 5. Discrete bubble train.

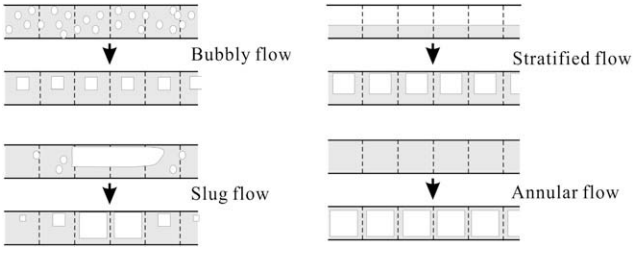

Fig. 6. Flow pattern image and corresponding discrete bubble model.

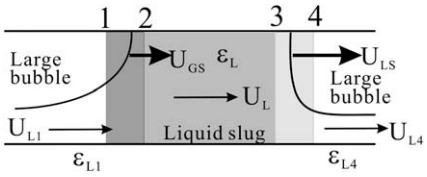

Fig. 7. Slug flow model, Ozawa et al. (1985).

effect of ascending bubble, a pressure drop, a slip relationship of bubble, and phase re-distribution over neighbouring cells due to the geometrical constraint.

Fig. 6 illustrates respective flow pattern in a horizontal flow and corresponding images of the discrete bubble model. In each image, the position of the bubble is slightly shifted towards upper boundary considering the actual phase distribution shown in Fig. 2, while the flow model is, in principle, one-dimensional, and thus the eccentricity of the bubble in the tube has no significance. The principal concept of this model is that actual bubbles are integrated or disintegrated to form a hypothetical bubble train so as to meet the requirement of the model. Then the large (or long) bubble in a slug flow is represented by a series of discrete bubbles along the tube as shown in Fig. 6, and annular flow is also represented by a bubble train with the highest void fraction. So far proposed model is for a vertical flow, and thus in application to a horizontal flow, at least the pressure jump condition across each cell and the slip relationship must be newly given so as to represent a principal feature of the horizontal flow.

The pressure jump condition is formulated based on the regime-based modeling of slug flow with well-known scooping–shedding mechanism of a liquid phase by Dukler and Hubbard (1975). This mechanism has been properly formulated by Ozawa et al. (1985), Ozawa and Sakaguchi (1985) and Sakaguchi et al. (1987) by applying Leibniz rule (Delhaye and Achard, 1976; Delhaye et al., 1981). Fig. 7 shows the flow model used in the analysis by Ozawa et al. (1985). The flow field is subdivided into a large bubble section (left side of 1 and right side of 4) and a liquid slug region (2-to-3). Boundary regions are set at each of liquid slug nose (3-to-4) and tail (1-to-2), through which liquid is scooped and shed, respectively. U_L, U_{L1} and U_{L4} represent liquid velocity in the slug, liquid velocities beneath the bubble at the slug tail and nose, respectively. The interface velocities, i.e. a large bubble velocity and a liquid slug velocity, are denoted by U_{GS} and U_{LS}, respectively. The hold-ups, i.e. liquid fraction ($\equiv 1-\varepsilon_G$), in the slug and of large bubble are denoted by ε_L, ε_{L1} and ε_{L4} as shown in Fig. 7. In formulating the momentum balance across the large bubble and the liquid slug, an accumulation of mass and momentum is ignored in the boundary regions, 1–2 and 3–4, so that the mass and momentum jump conditions are given by (Ozawa et al., 1985; Ozawa and Sakaguchi, 1985)

$$p_1 - p_2 = 0 \tag{3}$$

$$p_2 - p_3 = d(\rho_L \varepsilon_L U_L L_S)/dt + \Delta p_f + \varepsilon_L \rho_L U_L (U_L - U_{LS}) - \varepsilon_L \rho_L U_L (U_L - U_{GS}) \tag{4}$$

$$p_3 - p_4 = \varepsilon_{L4} \rho_L U_{L4} (U_{L4} - U_{LS}) - \varepsilon_L \rho_L U_L (U_L - U_{LS}) \tag{5}$$

where t denotes time, Δp_f a frictional pressure drop, L_S the liquid slug length, and suffixes 1–4 represent values corresponding to each boundary.

Eqs. (3)–(5) are, in principle, applicable to the large bubble and liquid slug system in a macroscopic framework, while we need cell-to-cell jump condition in the unit-cell system shown in Fig. 5. Then provided that these macroscopic relationships hold even in the present unit-cell system, and in addition under a quasi-steady assumption, the pressure jump condition across the unit cell is given by

$$p_i - p_{i+1} = \Delta p_f + \varepsilon_{L,i+1} \rho_L U_{L,i+1} (U_{L,i+1} - U_{G,i+1}) - \varepsilon_{L,i} \rho_L U_{L,i} (U_{L,i} - U_{G,i}) \tag{6}$$

It should be noted here that the nose velocity U_{GS} and the tail velocity U_{LS} in Eqs. (4) and (5) are assumed to be equal to the bubble velocity U_G under the quasi-steady hypothesis.

The pressure drop across the liquid part between two-successive bubbles are calculated as a single phase flow of liquid,

$$\Delta p_{fL} = \lambda \frac{D_p - D_b}{2D_p} \rho_L U_L |U_L|, \quad \text{where } \lambda = 0.3164 Re^{-0.25} \tag{7}$$

The friction factor λ is determined with the Blasius equation for turbulent flow based on the experimental evidence and the examined mass flux range (Reynolds number $Re \approx 4000$–$19{,}000$). The pressure drop across the annular part around the large bubble is given by (Wallis, 1969)

$$\Delta p_{fB} = 4\lambda_w \frac{D_b}{D_p} \frac{1}{2} \rho_L U_L |U_L|, \quad \text{where } \lambda = 0.005 \tag{8}$$

A hydrostatic pressure difference, i.e. a liquid height difference, affects the flow behavior, which becomes important in horizontal stratified and wavy flows. Then the equivalent static head H_{eq}, which is determined based on a holdup and the hydrostatic pressure distribution in the cross section (Sakaguchi et al., 1987), is introduced into Eq. (6) in calculating pressure difference (Ami et al., 2008) as

$$p_i - p_{i+1} = (\Delta p_{fL} + \Delta p_{fB}) + \rho_L g(\varepsilon_{L,i+1} H_{eq,i+1} - \varepsilon_{L,i} H_{eq,i})/2 + \varepsilon_{L,i+1} \rho_L U_{L,i+1} (U_{L,i+1} - U_{G,i+1}) - \varepsilon_{L,i} \rho_L U_{L,i} (U_{L,i} - U_{G,i}) \tag{9}$$

In a vertical flow focused in the previous papers (Ozawa et al., 2007; Ami et al., 2007), the slip velocity is given based on a balance between the drag and buoyancy forces exerted on a bubble, while in the horizontal flow model it is necessary to introduce alternative concept or equation as the local rule. In this paper, the slip velocity is determined with the help of gas cavity velocity in emptying of liquid-filled horizontal tube closed at one end (Zukoski, 1966). Benjamin (1968) analyzed such emptying process of liquid as a gravity current phenomenon and derived following relationship:

$$V_B / \sqrt{gD_p} = 0.542 \tag{10}$$

where V_B denotes the gas cavity velocity. This cavity velocity in a stationary liquid corresponds to the slip velocity u_r of the gas phase relative to the liquid phase. In a flowing liquid, as the momentum flux affecting on the cavity velocity is different from the stationary liquid, the cavity velocity, i.e. the slip velocity in the present case, is given by the modified formula by Weber (1981) and Sakaguchi et al. (1990) as

$$\frac{u_r}{\sqrt{gD_p \rho_{LG}/\rho_L}} = 0.542 - 1.76 Bd^{-0.56} \tag{11}$$

This equation implies that the slip velocity is not only a function of tube diameter, but also of the density difference and the surface tension. Below a certain limiting diameter, the slip velocity becomes zero, being well corresponding to the experimental observation of two-phase flow in a small-bore tube. Eq. (11) is thus applicable only to the tube diameter beyond $Bd = 8.19$, e.g. 1.574 mm at 5.0 MPa of CO_2. The zero cavity velocity corresponds to the case that emptying does not occur from the liquid-filled horizontal tube, i.e. phase stratification or phase-mal-distribution toward upper wall does not occur. Then the flow pattern tends to be axi-symmetric below $Bd = 8.19$. This critical value shown in Fig. 4 by dot-dash line is about twice the threshold of Kew and Cornwell (1997). It should be noted that the critical value $Bd = 8.19$ was obtained by extrapolation based on the experimental data with air–water and larger sized tubes. Thus the critical value may be modified and approach toward the critical value of Kew–Cornwell. Below this critical value, the slip

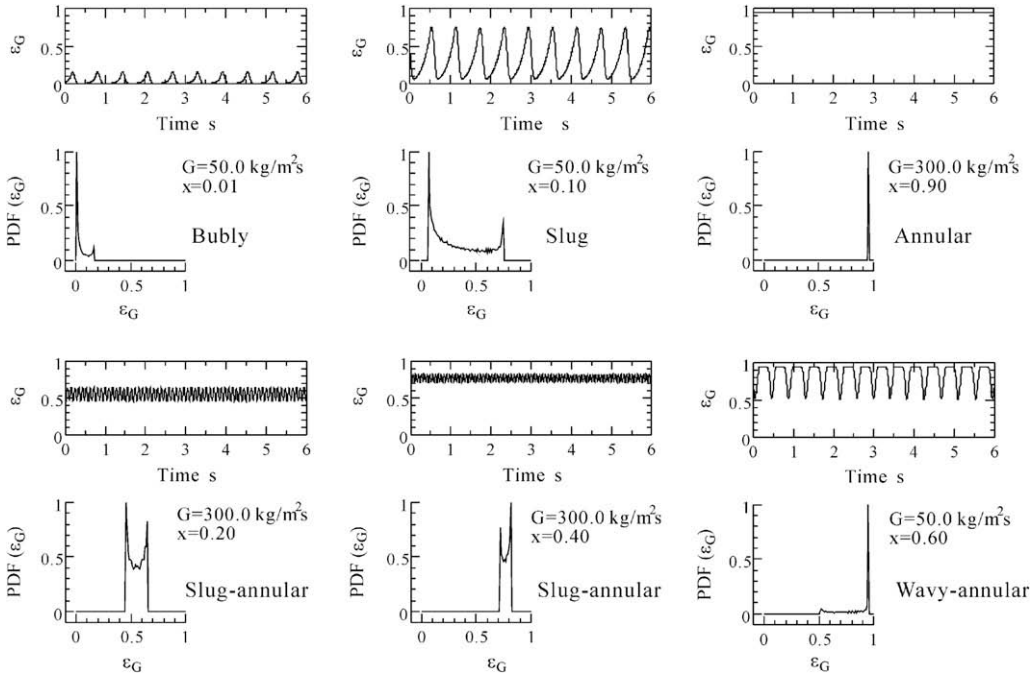

Fig. 8. Void fraction fluctuation and respective probability density function (PDF), p = 5.0 MPa, D_p = 2.0 mm.

velocity u_r is set at zero. Applying these relationships, the pattern dynamics simulation was conducted in the same manner as in the previous paper (Ozawa et al., 2007; Ami et al., 2007), where the other local rules and corresponding parameters or constants remain unchanged from the vertical flow model. The obtained results were statistically analyzed and the flow pattern was identified.

Fig. 8 shows typical void fraction fluctuation and respective probability density function (PDF) obtained in the pattern dynamics simulation. When the mass flux is low and the vapor quality is also low, small triangular waves appear (upper left column). The PDF represents almost single peak at very low void fraction. Increased vapor quality, the amplitude of the void fraction fluctuation increases and resultant PDF shows twin peaks at low and high qualities (upper middle). Further increase in the vapor quality is followed by almost constant void fraction and single peak at high quality (upper right). These three typical patterns correspond to bubbly, slug and annular flows, respectively. Such a feature is the same as in the vertical flow (Jones and Zuber, 1975; Ozawa et al., 2007; Ami et al., 2007). In the vertical flow simulation, churn flow, corresponding to slug-to-annular flow transition, appeared, while the void fraction fluctuation in the present horizontal flow is different from those in a vertical flow, i.e. void fraction has also fluctuation but is limited in an intermediate range of void fraction as shown in the first two figures in the lower column of Fig. 8. This flow pattern is considered as slug–annular flow in comparison with the experimental observation. In the case of low mass flux and relatively high vapor quality, another type of void fraction fluctuation, being limited in rather high void fraction range, appeared as in the last figure in the lower column. The highest void fraction in this pattern reaches the limited value predetermined in the simulation, and thus the geometrical configuration is considered as an annular flow but with very high waves on the liquid film. This pattern corresponds to the wavy–annular flow.

In the present discrete bubble model the highest void fraction is limited to 0.95, being reasonable for annular flow. In addition, the present model deals with the movements of discrete bubbles in the continuous liquid phase. Then droplets or entrainment of the liquid and perfectly separated flow are out of scope. Moreover the present model for horizontal flow takes into account the surface tension effect not in determining bubble geometry but in the slip velocity relationship. This makes it difficult to apply the present model to so-called "micro-channel" in the range less than Bd = 8.19, e.g. 1-mm and 0.5-mm tubes at 5.0 MPa (Yamamoto et al., 2007; Ozawa, 2009). In reality, the simulation conducted for 1-mm tube with u_r = 0 gave only an annular flow pattern. This discrepancy from the experimental observation shown in Figs. A1 and A3 may be improved by bringing a stability/instability mechanism due to surface tension and flow into the model, which is a future work left behind.

The flow pattern identification in the present simulation was based on the characteristic feature of PDF of the void fluctuation specified for each flow pattern as well as the following criteria:

Bubbly	$\varepsilon_{GL} < 0.1$, $\varepsilon_{GH} < 0.6$, mainly single peak.
Slug	$\varepsilon_{GL} < 0.1$, $\varepsilon_{GH} \geqslant 0.6$, twin peaks.
Annular	$\varepsilon_{GL} \geqslant 0.8$, single peak at highest void fraction.
Slug–annular	$0.1 < \varepsilon_{GL} < 0.8$, $\varepsilon_{GH} < 0.95$, twin peaks but is limited in an intermediate region of the void fraction.
Wavy–annular	$0.1 < \varepsilon_{GL} < 0.4$, $\varepsilon_{GH} \cong 0.95$, twin peaks but is limited in a narrow region of the void fraction.

where ε_{GL} and ε_{GH} denote minimum and maximum void fractions during the fluctuation, respectively.

The resultant flow pattern maps are shown in Fig. 9. The solid and dashed lines are the boundaries by Cheng et al. (2008) and Revellin et al. (2006) as in Fig. 3. Referring to the case of 2-mm tube, the flow pattern maps are, on the whole, in good agreement with the experimental results in Fig. 3, especially in regard to slug–annular and annular flows. In the simulation, plug flow is not identified, and is partly included in bubbly flow and the rest in slug flow. Then the bubbly flow regime is relatively wide compared with the experimental results. The wavy–annular flow region in the simulation is nearly consistent with the experiment, although the low mass flux condition was not fully examined in the experiments due to a limitation of experimental apparatus. The present simulation is inappropriate, as mentioned

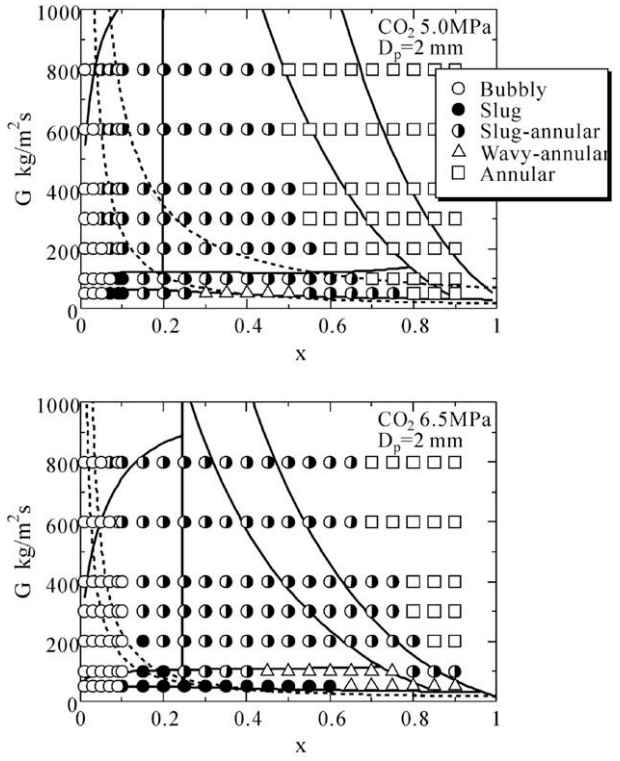

Fig. 9. Flow pattern map of 2-mm tube by simulation, solid lines: Cheng et al. (2008), and dashed lines: Revellin and Thome (2006), see Fig. 3 for legend of each region.

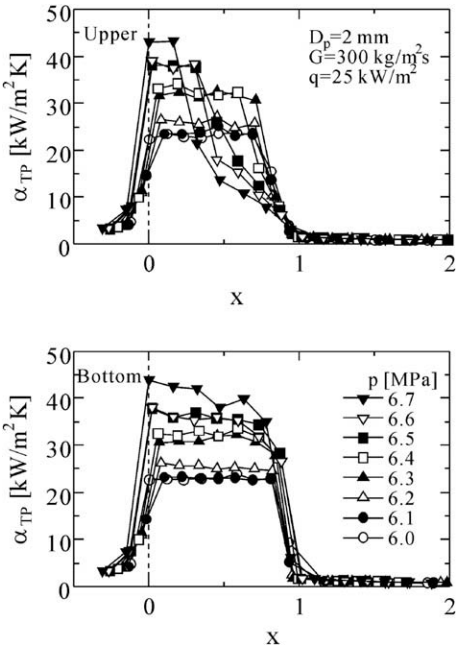

Fig. 10. Heat transfer coefficient at the upper and bottom walls of 2-mm tube.

above, to the perfectly separated stratified and wavy flows and the mist flow, and therefore these flow patters are not included in the maps of Fig. 9.

As mentioned above, the present discrete bubble model for horizontal flow is very effective in a rough estimation of the flow pattern. This model gives not only reasonable flow pattern prediction but also reasonable time-averaged properties of the void fraction and pressure drop (Ami et al., 2008). It is of course that such an application is limited, at this stage, in the macro-channels.

5. Intermittent dryout due to phase stratification

The phase stratification becomes significant at high pressure. When such flow pattern appears in a heated channel, the liquid film at the upper wall becomes essentially thin even in the case of low quality, which leads to the CHF at the upper wall while keeping nucleate boiling state at the bottom. This condition is referred to as "intermittent dryout" in the implication of alternative dryout and rewetting due to the intermittent flow, i.e. an inherent fluctuation of void fraction. Referring to the experimental results with 0.5-mm and 1-mm tubes (Yamamoto et al., 2007; Ozawa, 2009), the heat transfer coefficient is almost the same at both upper and bottom walls even in the intermittent flow patterns, except only a limited range of pressure and heat flux. This suggests that the vapor phase in the 1-mm or smaller tubes is weakly mal-distributed in the cross section, i.e. phase stratification is, if any, limited to a rather narrow region. Thus the critical heat flux (CHF) condition is brought about almost simultaneously both at the upper and bottom walls. On the other hand in 2-mm and 3-mm tubes, or 1-mm tube at higher pressure, e.g. 6.5 MPa, a remarkable temperature difference due to the partial and temporal dryout at the upper wall is anticipated due to the phase-stratification or phase-mal-distribution tendency observed in the flow pattern, e.g. in the slug and slug–annular flow.

Fig. 10 shows the heat transfer coefficients at the upper and lower walls of the 2-mm tube. The heat transfer coefficients at the upper and lower walls are almost constant against the quality increase, and are equal with each other in relatively low pressure region, namely below 6.4 MPa. This constant heat transfer coefficient indicates nucleate boiling being dominant. Beyond a certain critical quality, around 0.7–0.8 in this case, the CHF takes place and the heat transfer coefficient decreases drastically to a level of post-dryout heat transfer. Beyond 6.4 MPa, the heat transfer coefficient initiates to decrease moderately but at lower quality, i.e. the CHF initiates, at the upper wall. Further increase in the pressure results in a decrease in the critical quality. During such CHF at the upper wall, the lower wall is still at the nucleate boiling. In the 3-mm tube, the intermittent dryout takes place even at $p = 5.5$ MPa being lower than the 2-mm-tube case (Tanaka, 2009). This fact suggests that the phase-stratification tendency is much more significant in the 3-mm tube than in the 2-mm tube. It should be noted here that the heat transfer coefficients plotted in Fig. 10 are calculated with time-averaged values of wall temperature suffering from alternative dryout and rewetting. In reality, the tube wall of 2-mm tube was relatively thick, and the damping and phase lag of the temperature response was large so that the temperature fluctuation was hardly detected. On the other hand in the 3-mm tube, the temperature response was slightly improved, and the temperature fluctuation was clearly detected at the upper wall, while the bottom wall was kept at almost constant temperature (Tanaka, 2009).

The phase-stratification tendency is, as mentioned above, measured with the Bond number *Bd*. An increase in diameter from 2.0 mm to 3.0 mm corresponds to 2.25 times greater in *Bd*, and a increase in pressure from 5.0 to 6.5 MPa leads to 0.68 times in density difference, 0.24 times in surface tension, and thus 2.83 times in *Bd*. If the 1-mm tube is the case, *Bd* becomes 1/9 times of the 3-mm tube. In addition to the consideration on the Bond number, the liquid film dryout is a function of evaporation rate normal to the vapor–liquid interface, i.e. the heat flux, the mass flux, and the latent heat of vaporization, which are measured with the Boiling number *Bo* defined by $q/(Gh_{LG})$, where h_{LG} is a latent heat of vaporization.

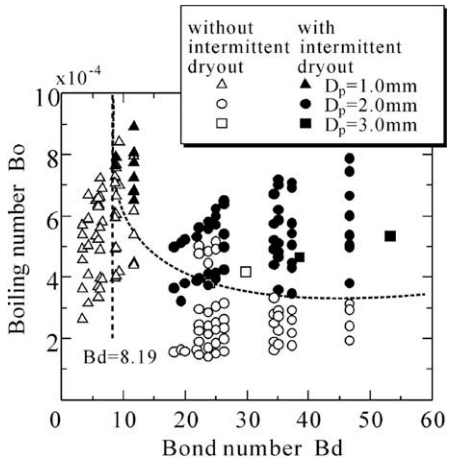

Fig. 11. Occurrence of intermittent dryout.

Fig. 11 shows the operating condition of the intermittent dryout as a function of the Bond and Boiling numbers based on the discrimination on the grounds of an appearance of heat transfer deterioration at the upper wall relative to the bottom wall. The plotted data includes those of 1-mm and 3-mm tubes. The vertical dashed line represents $Bd = 8.19$, the critical Bond number for phase stratification. Although the intermittent dryout would be a function of not only these two parameters but also the vapor quality and other parameters, the plotted data suggests that these two parameters, Bd and Bo, are available in rough prediction of an appearance of the intermittent dryout, i.e. the upper-right region beyond the dashed line confined by $Bd > 8.19$ and $Bo > 3.5 \times 10^{-4}$ in the present data.

The intermittent dryout tends to occur at high heat flux, and low mass flux condition. In addition, the heat transfer below the dryout quality is dominated by the nuclear boiling, being typically expected due to the fact that the heat transfer coefficient is an increasing function of the heat flux, and on the contrary a weak function of the quality. Provided a slug flow, being typical intermittent flow, when a liquid slug arrives, the upper wall is sufficiently wetted and thus the nucleate boiling takes place. When a large bubble with thin liquid film at the upper wall arrives, this thin liquid film is quickly dried out by the heat addition. Then the inner wall temperature increases drastically under the constant heat flux. The succeeding liquid slug then arrives at the reference position, and thus the dried-out wall is quenched again so that the nucleate boiling is recovered. As the liquid slug and the large bubble arrive alternatively, the measured temperature at the outer wall becomes a moderate value, i.e. an integral-averaged value due to the heat capacity and thermal diffusion of the tube wall. In order to formulate or to conduct phenomenological analysis on such intermittent dryout, it is preferable to make regime-based modeling, but not with the discrete bubble model. This is mainly because the present model is based on the one-dimensional hypothesis and thus is not suited to predicting geometrical configurations in three-dimension including phase-stratification phenomena.

6. Prediction of heat transfer coefficient during intermittent dryout

In order to simulate alternative dryout and rewetting during the intermittent dryou, it is preferable to use the slug flow model by Dukler and Hubbard's scooping–shedding mechanism (1975), being the most prominent and well-accepted one, i.e. the liquid slug is transported in a quite similar manner to a progressive wave.

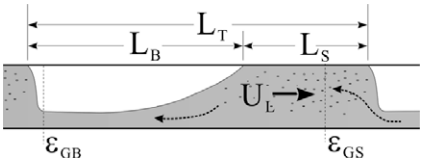

Fig. 12. Slug flow model with scooping–shedding mechanisms by Dukler and Hubbard (1975).

Fig. 12 demonstrates the slug flow model. The flow model is, in principle, the same as in Fig. 7. As to the geometrical configuration, L_S means the liquid slug length, a large bubble length L_B, and a quasi-steady slug flow, i.e. successively aligned slug unit of the length L_T, composed of a liquid slug and a large bubble, is provided. The time fractions of liquid slug and large bubble passing through a certain reference point are easily converted to the length fractions of liquid slug and large bubble, respectively, in quasi-steady state. Then the heat transfer coefficient is approximately given as the weighted-mean value of the heat transfer coefficient α_S in the liquid slug and post-dryout heat transfer coefficient α_B in the large bubble,

$$\alpha_{TP} = \alpha_S \frac{L_S}{L_T} + \alpha_B \frac{L_B}{L_T} \tag{12}$$

where the length L_T of the slug unit is given as a function of slug frequency f_S and the average velocity U_L of fluid in the slug (Dukler and Hubbard, 1975):

$$L_T = \frac{(1-r)U_L}{f_S} \tag{13}$$

$$U_L = \frac{G_L}{\rho_L} + \frac{G_G}{\rho_G} \tag{14}$$

G_L and G_G denote liquid and vapor mass fluxes, respectively, and r the scooping ratio, i.e. the ratio of scooped mass flow rate to the mass flow rate in the slug. The liquid slug length L_S is given by

$$L_S = \frac{U_L}{f_S(\varepsilon_{GB} - \varepsilon_{GS})}\left[\frac{G_L}{\rho_L U_L} - (1-\varepsilon_{GB}) + r(\varepsilon_{GB} - \varepsilon_{GS})\right] \tag{15}$$

where ε_{GB} and ε_{GS} denote the void fraction at the large bubble tail, and the void fraction in the slug, respectively. The scooping ratio r is given by Dukler and Hubbard (1975).

$$r = 0.021 \ln(Re_S) + 0.022 \tag{16}$$

where

$$Re_S = D_p U_L \frac{\rho_L(1-\varepsilon_{GS}) + \rho_G \varepsilon_{GS}}{\mu_L(1-\varepsilon_{GS}) + \mu_G \varepsilon_{GS}} \tag{17}$$

Then the large bubble length L_B is given by

$$L_B = L_T - L_S \tag{18}$$

Once the void fractions, ε_{GS} and ε_{GB}, are specified, these lengths are calculated. This, however, is not an easy task because of lacking suitable correlations and/or prediction methods. Thus in the present paper, both void fractions are given as input parameters so that the resulting heat transfer coefficient coincides to the experimental data.The heat transfer coefficient α_S in the slug is given by Schrock–Grossman-type correlation,

$$\frac{\alpha_S}{\alpha_{L0}} = K_1[Bo \times 10^4 + K_2 X^{-2/3}] \tag{19}$$

where X is the Martinelli parameter, and α_{L0} a single-phase heat transfer coefficient given by Dittus-Boelter's equation at the total mass flow rate as a saturated liquid. This hypothetical state is in a turbulent flow as mentioned above. The constants K_1 and K_2 are

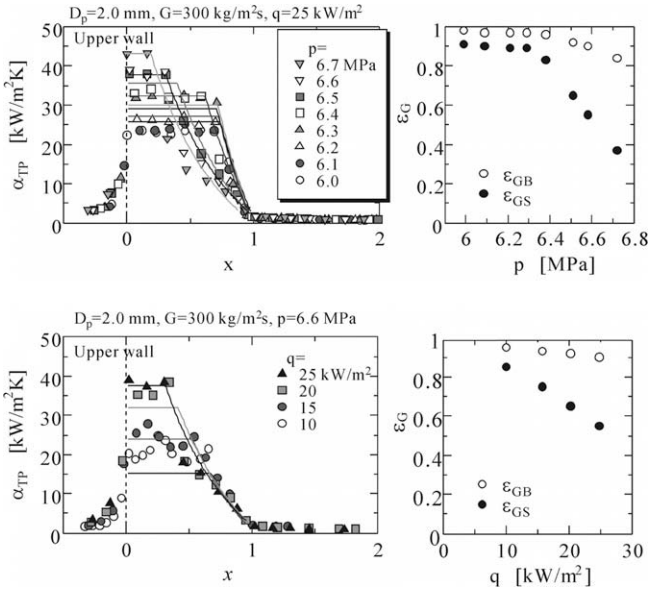

Fig. 13. Prediction of intermittent dryout at the upper wall of 2-mm tube, right column represents adopted void fractions.

determined so as to meet the data of the 2-mm tube, but retaining simple calculation as follows:

$$K_1 = 1.9, \quad K_2 = 0 \tag{20}$$

The disregard for convective component is due to the experimental evidence of the nucleate boiling being dominant. The post-dryout heat transfer coefficient α_B in the large bubble is given by Dougal and Rohsenow's correlation (1963), being easy to apply to the present calculation, although the accuracy is not verified and sophisticated model by Roko and Shiraha (1981) shows rather better agreement with the experimental data in the post-dryout region.

$$\alpha_B = 0.023 \frac{k_G}{D_p} \left[\frac{\rho_G G D_p}{\mu_G} \left(\frac{x}{\rho_G} + \frac{1-x}{\rho_L} \right) \right]^{0.8} Pr_G^{0.4} \tag{21}$$

where k_G is the thermal conductivity of gas, and Pr_G the Prandtl number of gas. In the course of calculation, if the slug length L_S exceeds the length L_T of the slug unit, L_S and L_B are set as

$$L_S = L_T, \quad L_B = 0 \tag{22}$$

and the heat transfer coefficient is given by

$$\alpha_{TP} = \alpha_S \tag{23}$$

The time-averaged heat transfer coefficient obtained in such a way is shown in Fig. 13, together with the specified void fractions in the liquid slug and at the large bubble tail (right side column). The horizontal line below the dryout quality given by Schrock–Grossman-type correlation, and the curves given by the present model are in good agreement with the experimental data. Thus the present regime-based modeling is effective in interpreting the possible mechanism of the phenomenon.

7. Conclusion

Experimental investigation on the flow pattern and boiling heat transfer of CO_2 in sub-critical pressure region was conducted with horizontal small-bore tubes of 1.0 mm, 2.0 mm and 3.0 mm in diameter. The phase stratification is significant even at high pressure with a small density difference, and thus the flow patterns observed in the tubes are consistent to those of the macro-channel, except 1-mm tube at 5.0 MPa which is close to the micro-channel. The observed flow pattern map suggests that the slug–annular flow occupies rather wide region penetrating into the annular flow region predicted by so far proposed criteria. This is also observed in the numerical simulation based on the pattern dynamics approach developed for a horizontal flow simulation.

The slug and slug–annular flows together with the effect of phase stratification leads to the intermittent dryout at the upper wall, while the bottom wall remains still a nucleate boiling state. Such an intermittent dryout has a close relationship with the Bond and the boiling numbers. With the help of the slug flow model by Dukler and Hubbard, the heat transfer coefficient during the intermittent dryout was examined, and the postulated heat transfer model was found to demonstrate the relevant mechanism.

Acknowledgements

This research work was in part conducted with the support of the Kansai University Research Grant: Grant-in-Aid for Joint Research, 2005. This work was also supported by JSPS. KAKENHI (19360104).

Appendix A

The flow patterns observed in 1-mm and 3-mm tubes are shown in Figs. A1 and A2, respectively, and the flow pattern maps are also shown in Figs. A3 and A4 for reference. Heat transfer data and detailed descriptions are found elsewhere (Yamamoto et al., 2007; Ozawa, 2009; Tanaka, 2009).

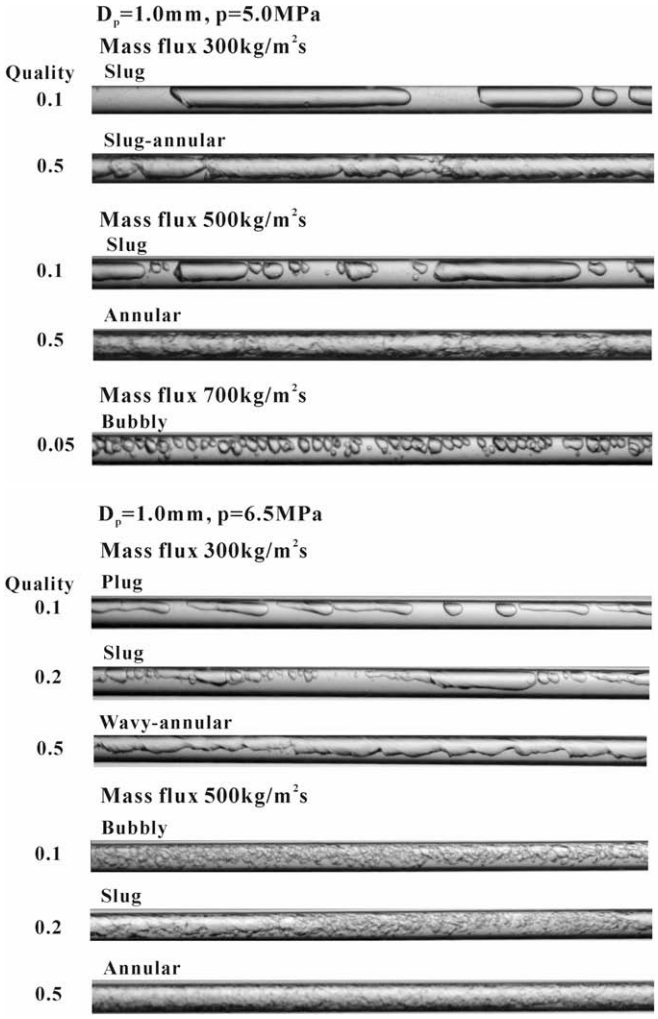

Fig. A1. Observed flow pattern of CO_2, D_p = 1.0 mm.

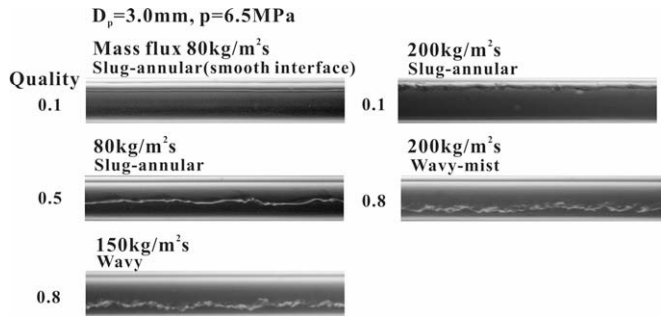

Fig. A2. Observed flow pattern of CO_2, D_p = 3.0 mm.

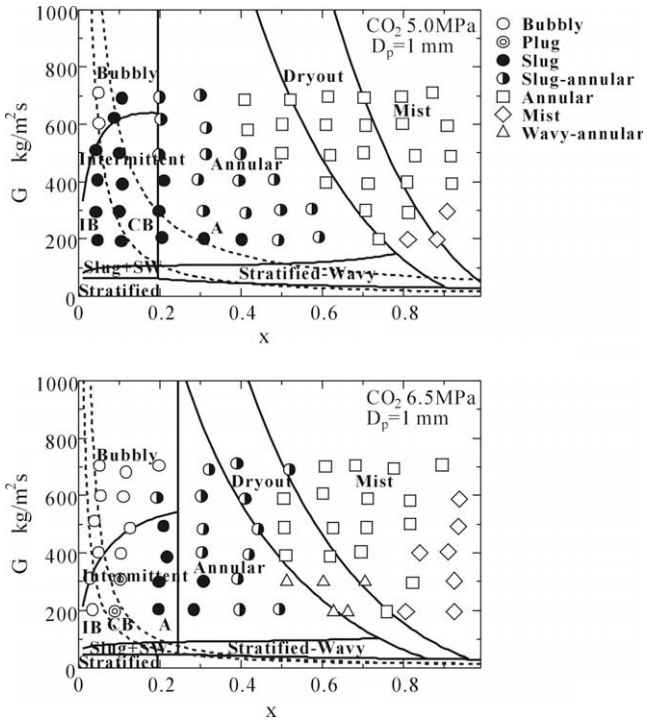

Fig. A3. Flow pattern map of CO_2 in 1-mm tube. Solid line: Cheng et al. (2008), and dashed line: Revellin and Thome (2006), IB: isolated bubble, CB: coalescing bubble, A: annular flow.

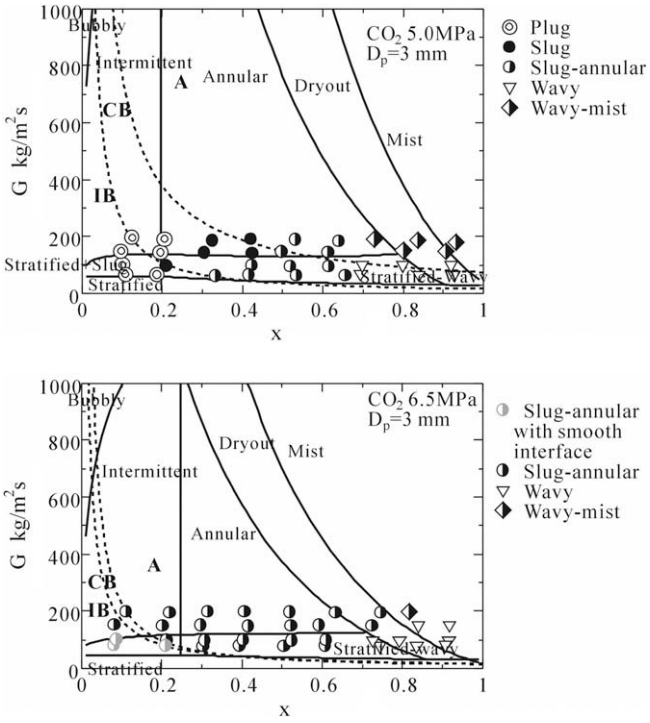

Fig. A4. Flow pattern map of CO_2 in 3-mm tube. Solid line: Cheng et al. (2008), and dashed line: Revellin and Thome (2006), IB: isolated bubble, CB: coalescing bubble, A: annular flow.

References

Ami, T., Umekawa, H., Ozawa, M., Shoji, M., 2007. Investigation on two-phase flow dynamics with discrete bubble model. Therm. Sci. Eng., 197–209.

Ami, T., Umekawa, H., Ozawa, M., Shoji, M., 2008. An application of discrete bubble model to horizontal two-phase flow. In: Proc. Int. Forum Heat Transfer, Paper No. 147, Tokyo.

Benjamin, T.B., 1968. Gravity current and related phenomena. J. Fluid Mech. 31, 209–248.

Cheng, L., Ribatski, G., Quiben, J.M., Thome, J.R., 2008. New prediction methods for CO_2 evaporation inside tubes: Part I – a two-phase flow pattern map and a flow pattern based phenomenological model for two-phase flow frictional pressure drops. Int. J. Heat Mass Transfer 51, 111–124.

Delhaye, J.M., Achard, J.L., 1976. On the averaging operators introduced in two-phase flow modeling. In: Proc. OECD Specialists' Meeting on Transient Two-Phase Flow, Toronto.

Delhaye, J.M., Giot, M., Riethmuller, M.L., 1981. Thermohydraulics of Two-Phase Systems for Industrial Design and Nuclear Engineering. Hemisphere, New York. Chapter 5, 95–116.

Dougall, R.S., Rohsenow, W.M., 1963. Film boiling on the inside of vertical tubes with upward flow of the fluid at low quality. MIT Heat Transfer Lab. Rep. 9079-26, Cambridge, MA.

Dukler, A.E., Hubbard, M.G., 1975. A model for gas–liquid slug flow in horizontal and near horizontal tubes. Ind. Eng. Chem. Fundam. 14, 337–347.

Jones Jr., O.C., Zuber, N., 1975. The Interrelation between void fraction fluctuations and flow patterns in two-phase flow. Int. J. Multiphase Flow 2, 273–306.

Kandlikar, S.G., 2002. Fundamental issues related to flow boiling in minichannel and microchannels. Exp. Therm. Fluid Sci. 26, 389–407.

Kandlikar, S.G., Grande, W.J., 2003. Evolution of microchannel flow passage – thermohydraulic performance and fabrication technology. Heat Transfer Eng. 24, 3–17.

Kattan, N., Thome, J.R., Favrat, D., 1998. Flow boiling in horizontal tubes: Part 3 – development of new heat transfer model based on flow pattern. J. Heat Transfer 120, 156–165.

Kew, P.A., Cornwell, K., 1997. Correlations for the prediction of boiling heat transfer in small-diameter channels. Appl. Therm. Eng. 17, 705–715.

Mishima, K., Hibiki, T., 1995. Effect of diameter on some characteristics of air–water two-phase flows in capillary tubes. Trans. JSME Ser. B, 3197–3204.

Ozawa, M., Sakaguchi, T., Hamaguchi, H., 1985. Gas–liquid two-phase transient slug flow modeling. Mem. Faculty Eng. Kobe Univ. 32, 1–23.

Ozawa, M., Sakaguchi, T., 1985. Note on modeling of transient slug flow in multi-phase flow system. Mem. Faculty Eng. Kobe Univ. 32, 25–44.

Ozawa, M., Ami, T., Umekawa, H., Shoji, M., 2007. Pattern dynamics simulation of void wave propagation. Multiphase Sci. Technol., 343–361.

Ozawa, M., 2009. Flow boiling of carbon dioxide in horizontal mini-channels and pattern dynamics approach to study flow pattern. In: Proc. 7th Int. ASME Conf. Nanochannels, Microchannels Minichannels ICNMM2009, Pohang, Keynote Papers No. 33-1.

Park, C.Y., Hrnjak, P.S., 2007. CO_2 and R410A flow boiling heat transfer, pressure drop, and flow pattern at low temperature in a horizontal smooth tube. Int. J. Refrigeration 30, 166–178.

Revellin, R., Thome, J.R., 2007. A new type of diabetic flow pattern map for boiling heat transfer in microchannels. J. Micromech. Microeng. 17, 788–796.

Roko, K., Shiraha, M., 1981. Post-dryout heat transfer in a vertical straight tube of a steam generator: 2nd report, approximate solutions. Trans. JSME Ser. B, 2014–2020.

Sakaguchi, T., Ozawa, M., Hamaguchi, H., Nishiwaki, F., Fujii, E., 1987. Analysis of the impact force by a transient liquid slug flowing out of a horizontal pipe. Nucl. Eng. Des. 99, 63–71.

Sakaguchi, T., Ozawa, M., Hamaguchi, H., Fukunaga, T., 1990. Behavior of a large bubble in a horizontal channel – 2nd report, large bubble penetrating into running liquid. Trans. JSME Ser. B, 1891–1898.

Schael, A.-E., Kind, M., 2005. Flow pattern and heat transfer characteristics during flow boiling of CO_2 in a horizontal micro fin tube and comparison with smooth tube data. Int. J. Refrigeration 28, 1186–1195.

Serizawa, A., Feng, Z., Kawara, Z., 2002. Two-phase flow and heat transfer in microchannels. Exp. Therm. Fluid Sci. 26, 703–714.

Tanaka, Y., 2009. Convective boiling and flow pattern of CO_2 in horizontal tubes. M.S. Thesis, Kansai University.

Thome, J.R., El Hajal, J., 2003. Two-phase flow pattern map for evaporation in horizontal tubes: latest version. Heat Transfer Eng., 3–10.
Thome, J.R., Ribatski, G., 2005. State-of-the-art of two-phase flow and flow boiling heat transfer and pressure drop of CO_2 in macro- and micro-channels. Int. J. Refrigeration 28, 1149–1168.
Thome, J.R., 2006a. Fundamentals of boiling and two-phase flow in microchannels. In: Proc. 13th Int. Heat Transfer Conference, Sydney, Keynote paper KN-14.
Thome, J.R., 2006b. State-of-art overview of boiling and two-phase flow in microchannel. Heat Transfer Eng., 4–19.
Triplett, K.A., Ghiaasiaan, S.M., Abdel-Khalik, A.I., Sadowski, D.L., 1999. Gas–liquid two-phase flow in microchannels. Part I: two-phase flow patterns. Int. J. Multiphase Flow 25, 377–394.
Weber, M.E., 1981. Drift in intermittent two-phase flow in horizontal pipe. Can. J. Chem. Eng. 59, 398–399.
Weisman, J., Duncan, D., Gibson, J., Crawford, T., 1979. Effects of fluid properties and pipe diameter on two-phase flow patterns in horizontal lines. Int. J. Multiphase Flow 5, 437–462.
Yamamoto, T., Ueda, Y., Ishihara, I., Ozawa, M., Umekawa, H., Matsumoto, R., 2007. Flow boiling heat transfer of carbon dioxide at high pressure in horizontal mini-channels. In: Proc. 6th Int. Conf. Multiphase Flow, ICMF 2007, Leipzig, S7-Wed-D-44 1-11.
Zukoski, E.E., 1966. Influence of viscosity, surface tension, and inclination angle on motion of long bubbles in closed tubes. J. Fluid Mech. 25, 821–837.